Near infrared adaptive optics flood illumination retinal angiography

ELENA GOFAS-SALAS,[1,2,3] PEDRO MECÊ,[1,3,4] LAURENT MUGNIER,[1] AURÉLIE MONTMERLE BONNEFOIS,[1] CYRIL PETIT,[1,3] KATE GRIEVE,[2,3,5] JOSÉ SAHEL,[2,4,5] MICHEL PAQUES,[2,3,5] AND SERGE MEIMON[1,3,*]

[1]*DOTA, ONERA, Université Paris Saclay, F-91123 Palaiseau, France*
[2]*Institut de la Vision, 17 rue Moreau, Sorbonne Universités, UPMC Univ Paris 06, INSERM, CNRS, 75012 Paris, France*
[3]*PARIS Group - Paris Adaptive-Optics for Retinal Imaging and Surgery, Paris, France*
[4]*Quantel Medical, Cournon d'Auvergne, France*
[5]*CIC 1423, INSERM, Quinze-Vingts Hospital, Paris, France*
[6]*Department of Ophthalmology, The University of Pittsburgh School of Medicine, Pittsburgh, PA, USA*
[*]*serge.meimon@onera.fr*

Abstract: Image-based angiography is a well-adapted technique to characterize vasculature, and has been used in retinal neurovascular studies. Because the microvasculature is of particular interest, being the site of exchange between blood and tissue, a high spatio-temporal resolution is required, implying the use of adaptive optics ophthalmoscopes with a high frame rate. Creating the opportunity for decoupled stimulation and imaging of the retina makes the use of near infrared (NIR) imaging light desirable, while the need for a large field of view and a lack of distortion implies the use of a flood illumination-based setup. However, flood-illumination NIR video sequences of erythrocytes, or red blood cells (RBC), have a limited contrast compared to scanning systems and visible light. As a result, they cannot be processed via existing image-based angiography methods. We have therefore developed a new computational method relying on a spatio-temporal filtering of the sequence to isolate blood flow from noise in low-contrast sequences. Applying this computational approach enabled us to perform angiography with an adaptive optics flood illumination ophthalmoscope (AO-FIO) using NIR light, both in bright-field and dark-field modalities. Finally, we demonstrate the capabilities of our system to differentiate blood flow velocity on a retinal capillary network in vivo.

1. Introduction

The accurate mapping and quantification of retinal blood flow has become a major goal in vision research since several of the most common retinal pathologies show vascular abnormalities as early symptoms, in particular at the microvascular level [1]. Different approaches have been explored to characterize the retinal blood flow. Doppler flowmetry, which uses speckle interferometry, was successfully used to generate maps displaying retinal perfusion and to extract the blood flow velocity, but with limited resolution [2, 3]. Other approaches such as image based angiography techniques, involving instruments such as Optical Coherence Tomography (OCT) or adaptive optics ophthalmoscopes, have been developed to achieve noninvasive visualization and characterization of retinal blood flow [4–6].

For all these systems, the computation of angiographic maps, known as motion contrast maps or perfusion maps, is based on the same principle. The blood is mapped by computing the temporal variance of an image sequence. This variance quantifies the variation in brightness generated by the absorption of the light by the passing erythrocytes. Through this computation a high signal appears where the blood passes. Among these non invasive technologies, OCT Angiography

(OCTA) competes in the clinical setting with the current gold standards of Fluorescein and Indocyanine Green angiography [7], both of these tests being invasive and requiring intravenous administration of a dye and long imaging sessions lasting from 10 to 30 minutes. OCTA has proven to be a fast and robust technique providing a 3D mapping of both the retinal and choroidal vascular network within a few seconds, showing both structural and blood flow information [8]. However, even though OCTA enables accurate mapping of large vessels, it has been shown that lumen sizes of smaller capillaries are generally overestimated [9, 10], which makes this technique less suitable to study the microvascular network than others with higher lateral resolution, such as ophthalmoscopes combined with adaptive optics (AO).

AO technology corrects the eye's aberrations in real time to capture images with diffraction-limited resolution [11]. Some teams have developed image processing to generate retinal perfusion maps adapted to image sequences obtained with AO corrected ophthalmosocopes, in both full field [5] and scanning configurations [12, 13]. Multiple studies have been carried out to study the retinal microvascular network, in particular in AO corrected scanning laser ophthalmoscopy (AO-SLO). Indeed, retinal perfusion maps where capillaries are accurately mapped [4, 14] were obtained thanks to the superior contrast and optical sectioning of AO-SLO compared to AO flood illumination ophthalmoscope (AO-FIO), and its combination with off axis techniques (eg dark-field, offset aperture, split detection). However, the scanning nature of the acquisition process in AO-SLO poses two problems when attempting quantitative angiography with this technique. Firstly, the presence of image distortion due to eye motion, even after post processing [15], generates artifacts in the contrast maps, and implies an uncertainty as to whether a movement observed between two frames is due to physiological reasons or due to scan distortion. Secondly, the AO-SLO acquisition rate is limited by the raster scan speed, which restricts the temporal resolution, making it difficult to accurately measure erythrocyte speed. Nevertheless some teams have been able to overcome this limitation through the manipulation of the scanning such as the multiple beam illumination carried out by DeCastro et al. [16], where the acquisition rate is increased over the scanning raster limit, enabling them to measure the speed of single erythrocytes in human retina in vivo. Other implementations such as the near confocal line scanning from Gu et al. [17] accelerates the scanning process as it is only carried out in one direction leading to images of blood flow in human parafoveal capillaries. Finally, another technique developed by Zhong et al. [18] achieves erythrocyte velocity by stopping the slow scanner leaving only a single line projected by the fast scanner on a blood vessel leading to spatiotemporal traces of erythrocytes. Although these solutions solve the temporal resolution limitations, they come with restrictions such as small field of view [18], an uneven contrast in capillaries [17] or a limitation concerning the direction and plane of the vessels whose blood flow can be analyzed [16].

In order to obtain the necessary spatial and temporal resolution, Metha's group developed an AO-FIO working at a wavelength centered at 593 nm and using a fast sCMOS camera (see Bedggood et al., [19]). The choice of this wavelength provides a near optimal erythrocyte contrast, leading to enhanced motion contrast maps. They studied neurovascular coupling at microvascular level with no distorsion and an accurate quantification of capillaries size as small as 3 μm. They measured the size of capillaries in reaction to stimulation and were able to detect less than a micron in variation [19]. However, the contrast maps obtained have a small field of view ($0.8° \times 0.2°$) which, for a larger analysis of the retina, would mean long imaging sessions. In addition, the use of a wavelength in the visible spectrum is not only uncomfortable for the subject, but for safety reasons, it restricts the amount of power that can be sent into the eye, which limits the size of the field of view. Finally, at this visible wavelength, the imaging light also stimulates the retina, so that stimulation and imaging cannot be decoupled.

It appears that there is an unanswered need for angiography maps produced from a flood illumination setup (providing distortion-free, large field-of-view, high frame rate sequences)

using Near Infrared (NIR) illumination (creating the opportunity for decoupled stimulation and imaging). However, flood-illumination NIR video sequences of erythrocytes, or red blood cells (RBC), have a limited contrast compared to scanning systems and visible light. As a result, although blood flow is visible in image sequences from our NIR AO-FIO [20], conventional image processing developed by the teams previously mentioned tends to fail in our image sequences due to a low signal-to-noise ratio (SNR). In this paper, we provide the methodology to produce NIR wide field undistorted angiography maps : we use a finely tuned NIR AO-FIO (previously described in [20]) to produce image sequences; we then use a temporal filter to isolate pixels which vary in contrast at a rate falling in the physiological range of erythrocyte velocity, and a spatial filter to reduce the noise variation; last, we compute perfusion maps from the filtered image sequences. This method is used on a few healthy subjects to test the method *in vivo*. Then, in order to validate our results we verified that the obtained angiography results are in line with previous works of the characterization of retinal blood flow. Finally, by temporally filtering the image sequence in various temporal bands, we demonstrate the capabilities of our system to map the blood flow velocity, opening the way to more elaborate and accurate velocity analysis of our data set.

2. Methods

2.1. Adaptive optics imaging

The imaging system used here is the PARIS AO-FIO which has been described in detail in a previous work [20]. The system consists of two optical subsystems, the Wavefront (WF) Sensing and Control subsystem and the Illumination and Detection subsystem (see schematic layout in Fig. 1). The dynamic and static aberrations of the eye are measured with a custom made Shack-Hartmann wavefront sensor and corrected using a 97 actuator deformable mirror (ALPAO, France). The adaptive optics loop rate is 50Hz. A fibered Super Luminescent Diode (SLD) (Omicron, Germany) with nominal center wavelength of 750 nm is used to measure the aberrations and an 860nm SLD (Omicron, Germany) coupled with a liquid fiber illuminates the retina with a 3.6° diameter field of view. The light is then back-scattered by the retina towards a fast Scientific CMOS ORCA flash4-V2 camera (Hamamatsu, Japan), enabling 2048×1024 pixel frame acquisition at 200Hz, which corresponds to $1.5\,\text{mm} \times 0.75\,\text{mm}$ field-of-view. The exposure time being set at 5 ms , acquired retinal images can be considered as distortionless, as eye movement can be considered negligible [21]. The magnification between the camera and the retina is such that each $6.5\,\mu\text{m}$ pixel corresponds to $0.73\,\mu\text{m}$ in the retina.

The camera is mounted on a motorized stage (Thorlabs, Germany) enabling us to focus on various layers of the retina by moving the stage.

2.2. Subjects

Healthy subjects were selected in order to compare our results to normal erythrocyte speeds in the literature. Acquisitions were made on two men (ages 28,39) and one woman (age 25). The project followed the tenets of the Declaration of Helsinki. Informed consent was obtained from subjects after the nature and possible outcomes of the study were explained. The subject's head was stabilized with a chin and forehead rest. They were asked to stare at the fixation target which enabled us to guide the subject's line of sight and explore various areas of the retina. The subjects pupil was not dilated. The total light energy entering the eye from the illumination source and the WFS source are respectively under $400\,\mu\text{W}$ and $2.8\,\mu\text{W}$, which is less than half the power stipulated by the ocular safety limits established by ISO standards for group 1 devices.
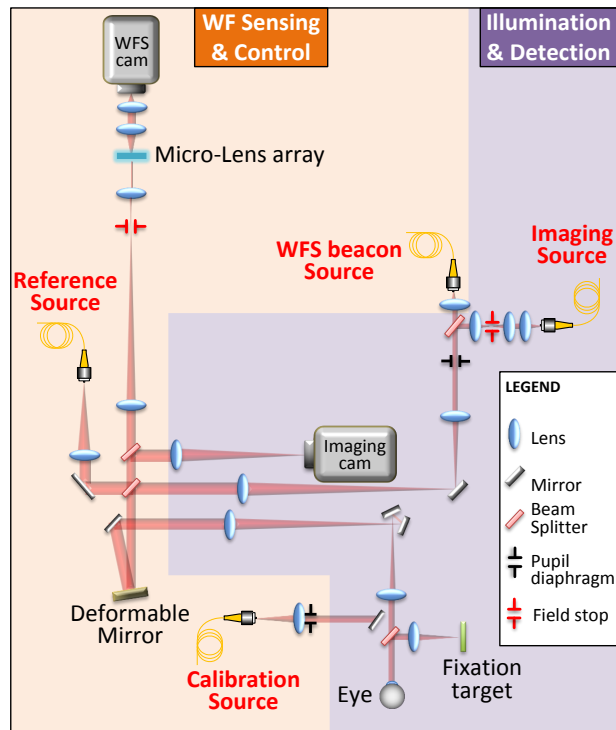
Fig. 1. Schematic drawing of the PARIS adaptive optics flood illumination ophthalmoscope.The system can be divided into two subsystems. Wavefront (WF) Sensing & Control, in yellow, is composed of a Reference Source (Ref Source), a Wavefront Sensor (WFS) (Micro-lens array, relay optics, and WFS camera), a WFS beacon source and a Deformable Mirror (DM). An additional calibration source can be inserted in place of the eye to calibrate the adaptive optics loop. The other subsystem, in purple, is Illumination & Detection and is composed of the retinal imaging camera and the corresponding wide field imaging source.

2.3. Image acquisition

AO-FIO image sequences of typically 1000 frames were acquired at 200Hz (total acquisition time of 4s) with a $2.7° \times 5.4°$ field of view.

For each subject we acquired image sequences near the lamina cribrosa ($10°$-$12°$) and the peripheral retina ($5°$-$10°$). In order to obtain optimal perfusion maps, the focus of the camera was placed on the nerve fiber layer. Images were acquired using standard bright-field AO-FIO illumination and dark-field AO-FIO illumination [22].

2.4. Image processing

2.4.1. Background subtraction and image registration

Following the acquisition, the low spatial frequency components of the retinal image, corresponding to scattered light from out of focus layers of the retina, were removed [20]. This correction was performed by subtracting a low-pass filtered version of each image from the raw image, where the low-pass image is obtained by a mean filter (kernel of 50 pixels) [23]. Then, the spatial variance was used as an image quality metric to get rid of images blurred [23] by fast and large fixational eye movements such as microsaccades or blinking. For each image sequence, about 1% of images were discarded, which represents so few frames that the temporal variance computation

leading to the perfusion maps is not affected. The final selected images were registered using a pairwise maximum likelihood sub-pixel approach [24]. An advantage of our method is that thanks to the high acquisition speed of our flood illuminated AO fundus camera, a single native image acts as template for stabilization of the acquired movies, without having to resort to an externally acquired template image as scanning techniques do [15] due to the distortion intrinsic to the scanning modality. The averages of the registered image sequences were computed.

2.4.2. Computation of perfusion maps

In order to isolate the signal variation produced by the absorption of erythrocytes flowing in vessels and capillaries, we developed a spatio-temporal filter with frequency bands centered on the theoretical spatial and temporal frequencies corresponding respectively to the size and speed of erythrocytes in retinal vessels. These filters were applied to the video frames before computing the temporal variance leading to enhanced contrast angiography maps of retinal vessels.

Temporal filtering - We start by applying a temporal filter to the image sequences. This enables us to get rid of signal variations slower than blood flow (e.g. deformation of the retina during the cardiac cycle) or faster than blood flow (high temporal frequency component of the noise).

We select a large frequency interval for the temporal filtering which goes from 10Hz to 80Hz, i.e. from 10% to 80% of the Nyquist temporal frequency of our instrument. The tuning of the frequency bandwidth was set to be as large as possible in order to avoid filtering erythrocyte motion while leading to the highest possible signal to noise ratio in perfusion maps. Processing was carried out in IDL programming language (IDL,Exelis,USA).

Spatial filtering - A spatial low-pass filter was then necessary to filter out the features, essentially noise, in the images whose variations fall in the same temporal frequency interval as the erythrocytes and therefore decrease the contrast of the motion contrast maps.

For the spatial filtering we used a Gaussian filter with a cutoff frequency (normalized by the Nyquist frequency) of 0.14, which corresponds to a spatial frequency of 47.6 cycles/mm. The boundary of the filter is chosen to filter structures smaller than 21 μm,which correspond to a few erythrocytes. As well as the temporal filtering the spatial cut-off frequency of the low pass filter was selected to increase the signal to noise ratio of the perfusion maps without filtering out blood cells.

Visualization 1 and Visualization 2 in Supplementary data are the registered image sequence (corresponding to the image presented in Fig. 2(C)) before and after the application of the spatio-temporal filtering. After this processing we obtain an image sequence containing only features around the size of a few erythrocytes moving at speeds close to the values of the blood flow speed.

Finally we compute the temporal variance of the sequence to obtain the motion contrast maps.

2.4.3. Perfusion color map generation based on blood flow speed

The high temporal resolution of the system allows us to subdivide the frequency band of the temporal filter in order to spatially analyze the different speeds of the retinal vessels. To achieve this, we apply various filters with different bandwidths to the video sequence and generate various contrast maps corresponding to each filter in order to be able to identify the capillaries and vessels with different blood flow speeds.

3. Results

3.1. *Perfusion maps in bright-field AO-FIO illumination*

Nonmoving structures are filtered out leading to enhanced contrast perfusion maps. Figure 2 shows two examples of typical perfusion maps obtained with NIR AO-FIO after spatio-temporal filtering in bright-field configuration. (A,C) are the average images of peripheral retinal vessels, (B,D) their corresponding perfusion maps. In all the images, large vessels lie in a nerve fiber bed where one can barely detect a hint of some capillaries. In the intensity images the capillaries are barely detectable, but appear with relatively high contrast in the perfusion maps. This ability to remove stationary features, such as the fibers signal, and enhance motion is shown in a magnified view (Fig. 2(A) and 2(B), yellow box). The red arrowheads in Fig. 2(C) and 2(D) indicate longitudinal capillaries going deep into the retina, these black spots in the average images appear as bright spots in the perfusion maps. Finally larger vessels remain visible in the perfusion maps (Fig. 2(B)). A magnified view (yellow box) in Fig. 2(D) shows the confluence of a venule with this vein. We observe multiple bands as if the flow remains unmixed after the confluence. See Visualization 2 and Visualization 3 in Supplementary in data to watch the videos corresponding to Fig. 2.
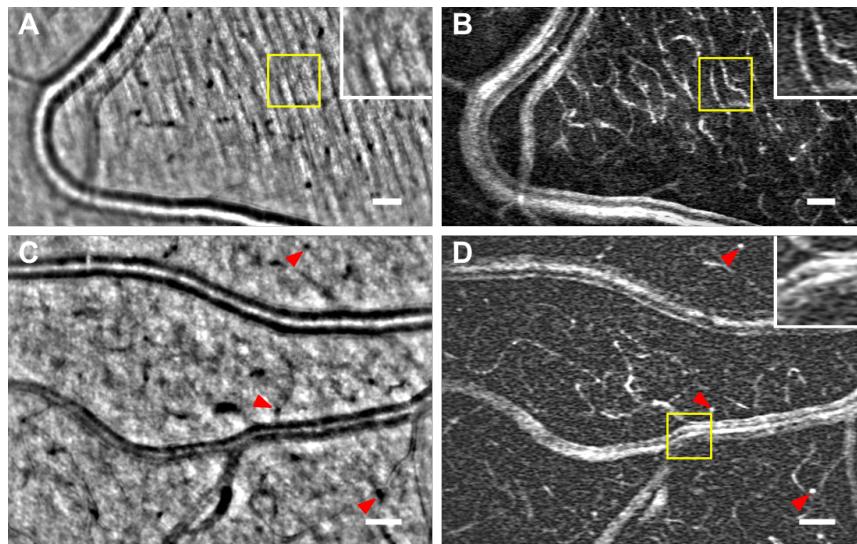

Fig. 2. (A,C) Average images of peripheral retinal vessels on the nerve fiber layer bed.(B,D) Motion contrast maps of the same areas displayed on the average images (see Visualization 1, Visualization 2 and Visualization 3 in Supplementary data). (C,D) show both an artery and a vein. In (A,B) A magnified view (yellow box) on the nerve fiber bed shows how the capillaries, invisible in the average image (A), appear contrasted on the perfusion map (B). In (C,D) Longitudinal capillaries, indicated with red arrowheads, in black in the average image (C) appear as bright white spots on the perfusion map (D). A magnified view (yellow box) in (D) shows in detail the confluence of the vein with a venule. The large vessel display several parallel bright bands, with the central band being the brightest. Scale bars are 50 μm
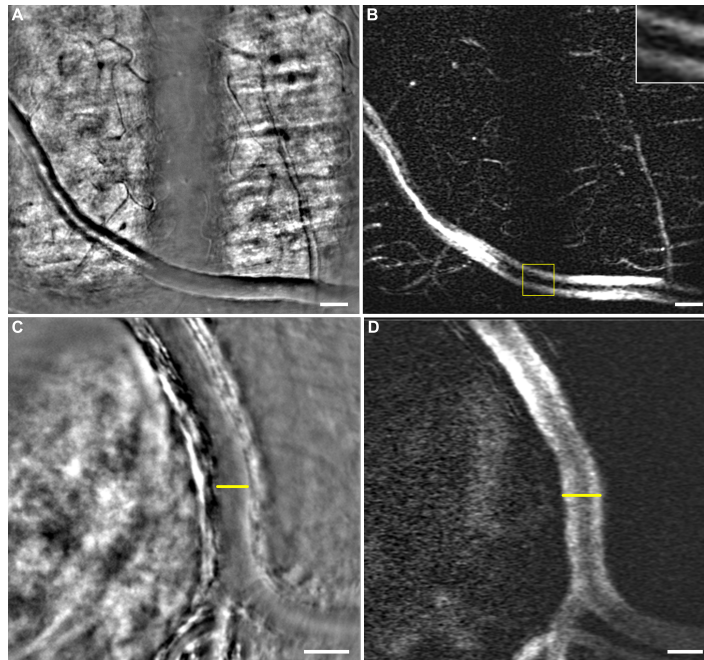
3.2. Perfusion maps in dark-field configuration

Fig. 3. (A,C) Average images including vessels with a contrast typical of dark-field modality and (B,D) their respective perfusion maps (see Visualization 4 and Visualization 5 in Supplementary data). (A) Large vessel of peripheral retina lying on the nerve fiber layer alternatively illuminated in bright-field and dark-field configuration. A magnified view (yellow box) in (B) shows the aspect of the perfusion map on a large vessel when illuminated in dark-field. The large vessel shows two parallel bands, with a darker aspect in the center of the vessel, instead of the typical several bands observed in bright-field configuration (cf. Fig 2(D)). Again, capillaries hardly visible in (A) appear contrasted in (B). (C) Artery from the optic nerve head region. The artery is lying over the lamina cribrosa which illuminates it from behind leading to forward scattering which gives this contrast to the vessel, characteristic of dark-field illumination. In (D) the large vessel lumen is easier to measure than in (C) where it is hard to determine the beginning of the wall (yellow lines). Scale bars are 50 μm

Since the use of the dark-field modality has enhanced perfusion maps in AO-SLO, we also acquired images in this illumination configuration and generated their respective perfusion maps. Figure 3 shows two average images of vessels with a typical dark-field configuration contrast Fig. 3(A) and 3(C). The dark-field illumination has been induced in Fig. 3(A) by introducing a field diaphragm in the illumination path while in Fig. 3(C) it is due to the presence of the lamina cribrosa located under the vessel [22]. Videos corresponding to these average images can be seen in Supplementary data Visualization 4 and Visualization 5. Figures 3(B) and 3(D) correspond to their respective perfusion maps. We observe in both of these maps that large vessels display two bands, with a darker aspect at the center of the vessel, instead of the several previously described in bright-field illumination, with a brighter signal in the center. A magnified view showing the aspect of the vessel on the dark-field area is displayed in Fig. 3(B) (yellow box). Another difference between perfusion maps in bright-field and dark-field configuration is the contrast of the capillaries. Indeed, the smaller capillaries seem to be less contrasted in the center of both bright and dark fields, while their contrast seems enhanced when they lie on the border between

the two different illumination fields.

3.3. Differentiation of vessels by blood flow speed

The high temporal resolution of the system enables a fine temporal sampling of the erythrocyte motion. The temporal filter, firstly designed to isolate the signal of red blood cell moving, is used here to separate this signal into three separate temporal bands going respectively from a frequency of 1Hz to 10Hz, 10Hz to 25Hz and 25Hz to 40Hz. This fractioned temporal filter was applied to an image sequence (corresponding to Visualization 6 in Supplementary data) acquired on a region with a capillary network to be able to compare blood speeds between several retinal vessels. Figure 4 shows, at the top, the average image of this region (Fig. 4(A)) and its corresponding perfusion map (Fig. 4(D)). At the bottom is presented the speed analysis with the three perfusion maps corresponding to these temporal bands Fig. 4(C), 4(D), 4(E). By assigning an RGB channel to each temporal frequency band, we generate a perfusion color map in which each color is associated to certain frequencies. In Fig. 4(F), blue represents the slower motions (1Hz to 10Hz), red the fastest (25Hz to 40Hz), while green is used to display features moving at medium speeds (10Hz,25Hz). We notice that although the three perfusion maps share many similar features, some capillaries appear more clearly in one particular map than another. Indeed this difference is highlighted in color map Fig. 4(F). For instance, capillaries appearing contrasted in Fig. 4(C) while invisible in 4(D) and 4(E) are blue in image 4(F).
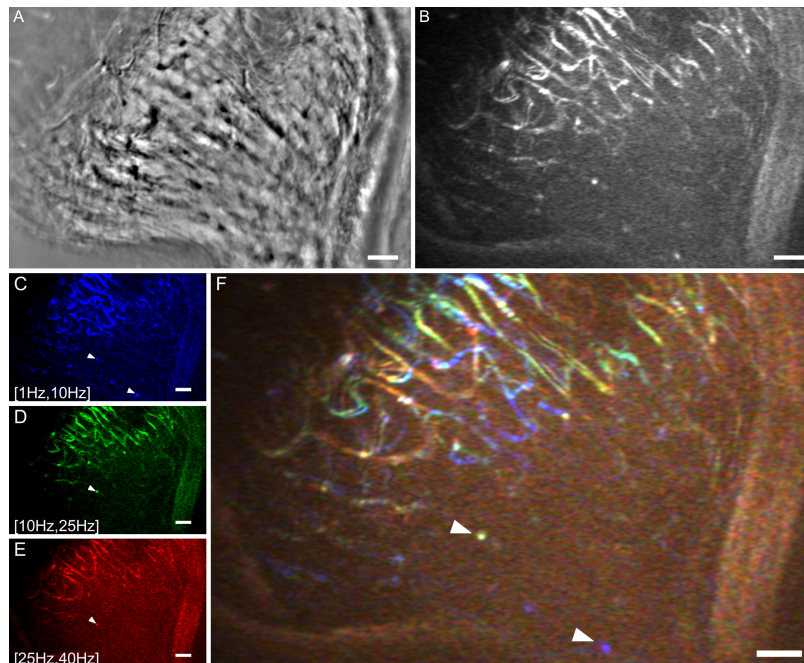

Fig. 4. (A) Average image of a capillary bed near the lamina cribrosa region and (B) its respective perfusion map after a temporal filtering with a frequency bandwidth of [1Hz,40Hz] (see Visualization 6 in Supplementary data). (C,D,E) Perfusion maps of that same region after three different temporal filtering, with respectively frequency bandwidths of [1Hz,10Hz] (blue map),[10Hz,25Hz] (green map) and [25Hz,40Hz] (red map). (E) Perfusion color map generated by assigning to each perfusion map from a temporal frequency band (A,B,C) an RGB color. Slow temporal frequencies are in blue, medium in green and the faster frequencies corresponds to red. White arrowheads indicate two examples of longitudinal capillaries. Scale bars are 50 μm.

In each channel sub-image Fig. 4(C), 4(D) and 4(E), the pixels appearing bright are pixels temporally varying with frequencies between [1Hz,10Hz], [10Hz,25Hz] and [25Hz,40Hz] respectively.

4. Discussion

4.1. Distortionless high resolution perfusion maps in the near infrared

Distortionless high resolution perfusion maps in near infrared could be a highly valuable tool for assessing the state of the retinal vascular network, and particularly for neurovascular studies of the retina, as near infrared wavelength range is more confortable for the subject, safer in terms of thermo-chemical damage, and does not stimulate the retina (thus enabling decorrelation of stimulation and imaging channels to carry out functional imaging). Distortionless maps would enable extraction of reliable biomarkers, such as foveal avascular zones (FAZ) [12]. Such maps can only be obtained using adaptive optics (for spatial resolution) near-infrared imaging, in a full-field modality (to prevent distortion artifacts entailed by scanning), such as the PARIS AO-FIO [20]. Indeed, there are two main difficulties generated by the distortion artifacts, which are produced in an image obtained with a retinal scan when the eye moves during the acquisition of a frame. On the one hand, when there is a deformation in a retinal structure, there is an uncertainty regarding whether it comes from distortion or has physiological origin. On the other hand, to correct distortion on all the frames in an image sequence, the user must select a reference frame. However, there may not be a working reference in every acquisition [15]. Although some teams have found solutions to increase the acquisition rate of scanning systems and therefore minimize the impact of eye movement [18], choice of template remains subjective, meaning that the metrics extracted from processed images could be confounded by significant local distortions, caused for instance by disease. In consequence, some teams resort to using an image acquired sequentially with an AO fundus camera as a ground truth template for distortion correction [15]. Our images, acquired with a high speed AO fundus camera, are inherently ground truth templates and thus distortion free allowing reliable metric extraction. However, the existing perfusion map processing methods, which produced either high contrast maps in near-infrared contrast maps with distortion [12, 13] , or without distortion but in another wavelength (wavebands centered on 593nm to maximize erythrocyte absorption contrast [5, 19]), fail in full-field NIR due to a poorer SNR in the image sequences. Using a spatial and temporal filtering of our image sequences, we were able to obtain large field-of-view (2.7°× 5.4°) distortion-free enhanced contrast perfusion maps of the retina using AO-FIO image sequences in near infrared. The spatial resolution (down to capillaries of 5 μm $\pm$ 1 μm diameter) and contrast (0.6-0.8 range) of the obtained perfusion maps is similar to confocal AO-SLO results [14].

A thorough analysis of the image sequences was carried out in order to confirm that the perfusion maps were not a result of introduced artifacts by the filter: when looking at bright-field perfusion maps we notice that large vessels display parallel bands with, in several cases, a brighter central band. We first thought that this brighter central band could be due to the temporal variation of the specular reflection along the crest of the vessel wall instead of erythrocyte motion. However, when closely looking at the videos (http://www.fox5dc.com/news/local-news/video-bear-spotted-in-montgomery-county, image sequence corresponding to average Fig. 2(C)) we observe a flow motion at the center of the vessel with a speed and direction close to the blood flow characteristics, leading us to the conclusion that the bright band at the center of the large vessel in the perfusion map is generated by a temporal variation of erythrocytes motion.

Finally, to validate our results we verified that the obtained perfusion maps are in line with previous works of the characterization of retinal blood flow: Fig. 2(D) shows a vein on the lower part of the image with several ramifications. The flux seems to remain unmixed after the confluence as we observe these various bands in the perfusion map. Indeed, this phenomenon has been previously described in [14] using AO-SLO where they show perfusion maps of several

branch venules entering a vein with various illumination configurations.

4.2. Comparing dark-field and bright-field perfusion maps

Our system enables us to acquire dark-field and bright-field images in AO-FIO of the same regions [22]. We wanted to verify if the dark-field modality in flood imaging could increase the contrast of the perfusion maps the same way it has been shown in AO-SLO [14].

With regards to capillaries in perfusion maps, Chui et al report enhanced contrast in dark-field imaging with AO-SLO [14]. In our case, for instance in Fig. 3(B), capillary contrast is higher in the bright-field zone than in the dark-field zone, except at the edge of the central obscuration. This zone, which corresponds to the maximal illumination gradient in the image, is precisely the region where the sensitivity to the phase of the sample is the highest [25] and where the dark-field full-field configuration most closely resembles the standard scanning configuration [14].
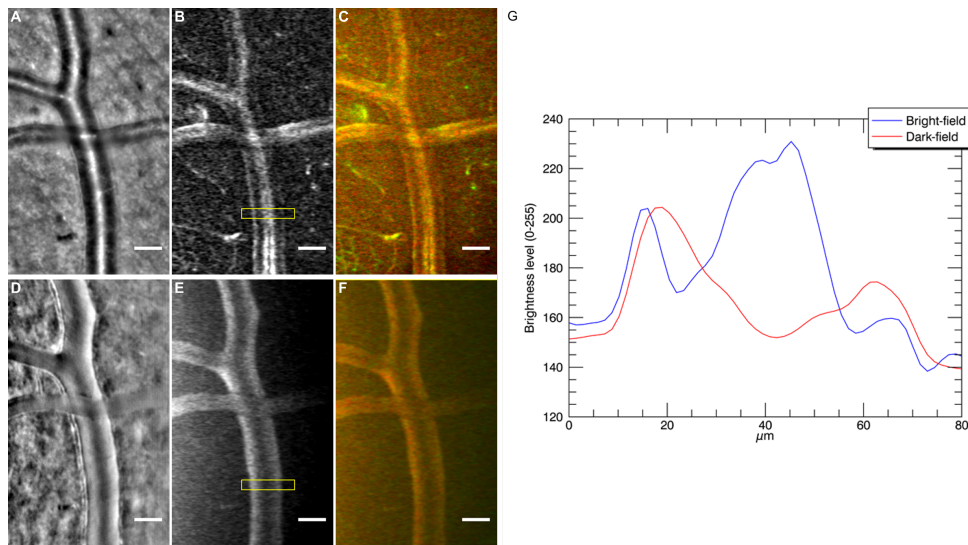

Fig. 5. Images generated from image sequences of the same region showing an artery crossing with a vein in bright-field (A,B,C) and dark-field (D,F,E) illumination configuration respectively (see Visualization 7 in Supplementary data). (A,D) are average images, (B,E) perfusion maps and (C,F) color generated maps showing in green slow variations and in red fast variations. (G) displays two horizontal intensity profile plots (vertically averaged) from yellow boxes in images (B) and (E) corresponding to bright-field and dark-field perfusion maps respectively. The x-axis indicates the horizontal position in microns inside the yellow box and the y-axis indicates the brightness level of the vertical average for each of these horizontal positions.

With regards to larger vessels, we acquired image sequences of the same region, showing an artery crossing with a vein, in bright-field and dark-field (see Visualization 7 in Supplementary data). In addition to the fact that average images in bright-field and dark-field show differences in contrast (Fig. 5 (A), 5(D)), we also noticed that perfusion maps in both configurations show significant differences. In Fig. 3, we noticed that large vessels display only two parallel bands in dark-field perfusion maps, whereas several bands are visible in our bright-field configuration. The same effect is shown in Figs. 5(B) and 5(E), where we show the perfusion maps of the same region for comparison purposes. The corresponding intensity profiles are plotted in Fig. 5(G): the blue plot, corresponding to the bright-field map, has three maxima (three bands), with the

central maximum higher than the ones on the sides; the red plot, corresponding to the dark-field map, has only two maxima, with a darker region in the center of the vessel.

It is interesting to note that this two line shape observed in dark-field modality in full field is not observed in the dark-field modalities perfusion maps shown in [14]. This could be due to the fact that AO-SLO offset aperture dark-field modality does not completely filter the single back-scattered light, leading to images with a slight back-scattered reflection on top of the lumen of the larger vessels.

The flow shape observed in our system dark-field illumination seemed to imply that erythrocytes have two preferred paths that lie on each side of the lumen, which was in contradiction with the observations made on bright-field perfusion maps (showing several bands). However, when studying the flow in image sequences with dark-field configuration, we are able to detect at times the blood flow motion in the center of the vessel (see Visualization 4 corresponding to the video from Fig. 3(A)) which goes against this hypothesis of two preferred paths. Our interpretation of this discrepancy is illustrated in Fig. 6. Let us consider first the bright-field case. In the same way in which the specular reflection will be greater at the top of the vessel where the wall is orthogonal to the direction of illumination, the back-scattering generated by the inside of the lumen of the vessel will also be greater on the wall that is orthogonal to the direction of the illumination, leading to more photons returning in this direction to the camera (see left image in Fig. 6). Thus, the variation in intensity would be greater along the crest of the vessel wall orthogonal to illumination than in other areas of the vessels which back-scatter relatively less light. The variance signal would therefore be higher at the center than the borders, and thus the variance image would be brighter.

In dark-field, the light detected by the camera comes from forward scattering (scattered by layers below the artery) and goes through the vessel, where it is partially absorbed by red blood cells flowing inside the vessel. The absorption is then stronger at the center, where the vessel (and red blood cell flow) is the thickest. In dark-field, this effect is not counterbalanced by a stronger specular reflection at the bottom of the vessel, so that no bright central band is visible.
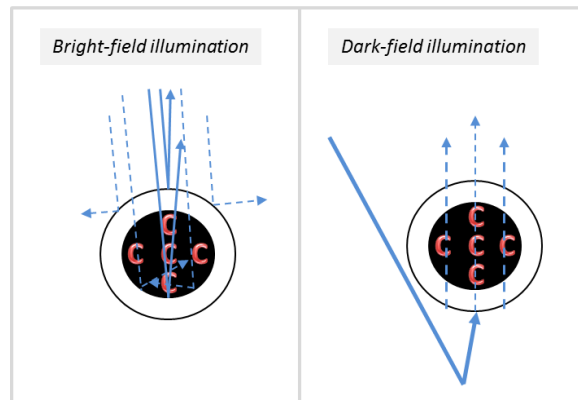

Fig. 6. Schematic drawings showing a cross-section of a vessel scattering light in bright-field (left) and dark-field (right). The red C letters represent red blood cells (or erythrocytes) and blue arrows represent light rays, dashed lines representing lower amount of photons while the solid lines show larger amounts.

4.3. Wall-to-lumen ratio

Aside from studying perfusion itself, a better estimation of the size of the lumen can be reached with perfusion maps, leading to more accurate retinal biomarkers such as wall-to-lumen ratio [26]

or quantification of vessel lumen expansion or contraction [19]. Indeed, perfusion maps of vessels enable us to determine their lumen size better than in averaged reflectance images, because they mark the passage of the blood, and therefore display the lumen size of capillaries and veins more distinctively. For instance, Figs. 3(C) and 3(D) show how the limit between lumen and wall is hardly distinguishable in 3(C) while the perfusion map 3(D) displays a sharp border between the high bright signal coming from the blood flow motion and the dark background coming from the motionless vessel wall.

4.4. Velocity color maps

Figure 4 shows how by applying a temporal filter to the image sequence with various cut off frequencies we can identify capillaries with different blood flow speeds. Indeed when we assign a color to each temporal band and we merge them in one image (Fig. 4(F)), we observe that the capillary network displays a mixture of these three colors. This means that two pixels with different colors vary at different speeds. In particular we observe that the longitudinal vessels (indicated with white arrowheads in Fig. 4), which are not visible in AO-SLO [14], display a slower signal variation than other capillaries whose flow moves laterally. By using simplistic assumptions, it is possible to link the pixel temporal variation with an order of magnitude of the blood velocity. We assimilate the red blood cells as particles with a typical size ϕ_{RBC}, and we suppose that these particles have a periodic flow with a spatial period equal to $2\phi_{RBC}$, so that the blood flow speed v_{RBC} is linked to the pixel temporal frequency v as:

$$v_{RBC} = 2\phi_{RBC} \cdot v \tag{1}$$

It is difficult to assign an accurate value to ϕ_{RBC}: red blood cells can get as small as 5 μm when they fold to travel in small capillaries [27, 28]; on the other hand, the particles we visualize in video sequences often correspond to a cluster of red blood cells rather than individual ones, with a typical size around 20 μm. We will consider here an 8 μm typical value [5]. With this simplistic model, the three inferred velocity ranges corresponding to Fig.4(F) frequency bands are [0.02 mm/s,0.2 mm/s], [0.2 mm/s,0.5 mm/s] and [0.5 mm/s ,0.8 mm/s]. These orders of magnitude are in agreement with the literature [5]. Although this approach only provides an order of magnitude of the absolute blood velocity, it does provide insight on the relative blood velocity in the vascular network. For instance, capillary velocity maps such as Fig.4(F) could be used to monitor blood flow abnormalities at a microvascular level.

4.5. Limitations and future work

A limitation from this temporal analysis appears in Figs. 5(C) and 5(F). This cropped area of a color map displays in the same red color a vein and an artery crossing, even though arterial flow is faster than the blood flow in veins. This could be caused by the fact that we analyzed the intensity variation caused by the RBC passage over a large temporal interval (a few seconds), which is longer than a diastole and systole (less than a second), leading to the averaging of the artery speed variations. We would need to increase the temporal resolution to reach a rate higher than the current rate of our system (200Hz) and analyze over a smaller interval, which requires a more powerful light source so as not to limit the SNR, and a faster camera. Also, some small artifacts appear in the form of white lines parallel to the vessel walls, which we interpret as the temporal variation of the vessels vibrating when the blood is flowing.

Despite these limitations, the technique presented here opens up exciting prospects, such as producing 3D dark-field angiography maps. In Fig. 2 three examples of this vessel going into deeper retina layers are indicated with red arrowheads in both the average image Fig. 2(C) and its perfusion map Fig. 2(D). These longitudinal vessels and capillaries do not seem to appear to our knowledge in AO-SLO images, and belong to the vascular plexus linking the various vascular

beds. The detection and mapping of these vessels could lead to the possibility of 3D mapping the microvascular network the same way OCT does for the larger vascular network. Indeed, we have recently shown that the axial resolution capabilities of our AO-FIO system are better than usually accounted for in the literature, and that cross sectional images (analoguous to OCT B-scans) can be produced to identify the various retinal layers [29]. The combination of this tool with the undistorted widefield angiography maps (in dark-field or bright-field) presented here could lead to the 3D mapping of the microvascular network.

Future work will be oriented towards improving the spatial dynamic study of the perfusion and increasing the accuracy of the blood flow speeds in capillaries by increasing the acquisition rate and/or developing more sophisticated processing to derive the erythrocytes' speeds in a similar way to particle image velocimetry [30].

5. Conclusion

The high spatial and temporal resolution of the NIR AO-FIO combined with the specific image processing presented in this paper enables us to compute retinal perfusion maps with enhanced contrast, no distorsion and a large field of view. In particular, we are able to resolve capillaries as small as 5 μm in various regions of the retina. These angiography maps obtained on healthy subjects are in line with the characteristic described in previous work of the field validating this image processing method. The implementation of the dark-field illumination in full field led to an increase of contrast at the boundary between the illuminated and dark areas in perfusion maps. This observation encourages us to compute motion contrast maps with different structures of the illumination in order to further improve the contrast of these maps. Another valuable feature of our system, possible because of the high acquisition rate, is the spatial analysis of the temporal dynamic of the blood flow. By temporally filtering the image sequence we can generate several perfusion maps, each one showing capillaries with blood flowing at a different speed range.

Funding

Disclosures

The authors declare that there are no conflicts of interest related to this article.

References

1. T. Bek, "Regional morphology and pathophysiology of retinal vascular disease," Prog. Retin. Eye Res. **36**, 247–259 (2013).
2. G. Michelson, J. Welzenbach, I. Pal, and J. Harazny, "Automatic full field analysis of perfusion images gained by scanning laser doppler flowmetry," Br. J. Ophthalmol. **82**, 1294–1300 (1998).
3. R. D. Ferguson, D. X. Hammer, A. E. Elsner, R. H. Webb, S. A. Burns, and J. J. Weiter, "Wide-field retinal hemodynamic imaging with the tracking scanning laser ophthalmoscope," Opt. Express **12**, 5198–5208 (2004).
4. T. Y. Chui, S. Mo, B. Krawitz, N. R. Menon, N. Choudhury, A. Gan, M. Razeen, N. Shah, A. Pinhas, and R. B. Rosen, "Human retinal microvascular imaging using adaptive optics scanning light ophthalmoscopy," Int. J. Retin. Vitreous **2**, 11 (2016).
5. P. Bedggood and A. Metha, "Direct visualization and characterization of erythrocyte flow in human retinal capillaries," Biomed. Opt. Express **3**, 3264–3277 (2012).
6. Z. Mammo, C. Balaratnasingam, P. Yu, J. Xu, M. Heisler, P. Mackenzie, A. Merkur, A. Kirker, D. Albiani, K. B. Freund, M. V. Sarunic, and D.-Y. Yu, "Quantitative noninvasive angiography of the fovea centralis using speckle variance optical coherence tomography," Investig. Ophthalmol. & Vis. Sci. **56**, 5074 (2015).
7. R. F. Spaide, J. M. Klancnik, and M. J. Cooney, "Retinal vascular layers imaged by fluorescein angiography and optical coherence tomography angiography," JAMA Ophthalmol. **133**, 45–50 (2015).
8. Y. Jia, J. C. Morrison, J. Tokayer, O. Tan, L. Lombardi, B. Baumann, C. D. Lu, W. Choi, J. G. Fujimoto, and D. Huang, "Quantitative oct angiography of optic nerve head blood flow," Biomed. Opt. Express **3**, 3127–3137 (2012).

9. T. S. Hwang, S. S. Gao, L. Liu, A. K. Lauer, S. T. Bailey, C. J. Flaxel, D. J. Wilson, D. Huang, and Y. Jia, "Automated quantification of capillary nonperfusion using optical coherence tomography angiography in diabetic retinopathy," JAMA Ophthalmol. **134**, 367–373 (2016).

10. A. M. Hagag, S. S. Gao, Y. Jia, and D. Huang, "Optical coherence tomography angiography: technical principles and clinical applications in ophthalmology," Taiwan J. Ophthalmol. **7**, 115 (2017).

11. J. Liang, D. R. Williams, and D. T. Miller, "Supernormal vision and high-resolution retinal imaging through adaptive optics," JOSA A **14**, 2884–2892 (1997).

12. T. Y. Chui, Z. Zhong, H. Song, and S. A. Burns, "Foveal avascular zone and its relationship to foveal pit shape," Optom. Vis. Sci. **89**, 602 (2012).

13. J. Tam and A. Roorda, "Speed quantification and tracking of moving objects in adaptive optics scanning laser ophthalmoscopy," J. Biomed. Opt. **16**, 036002 (2011).

14. T. Y. Chui, D. A. VanNasdale, and S. A. Burns, "The use of forward scatter to improve retinal vascular imaging with an adaptive optics scanning laser ophthalmoscope," Biomed. Opt. Express **3**, 2537–2549 (2012).

15. A. E. Salmon, R. F. Cooper, C. S. Langlo, A. Baghaie, A. Dubra, and J. Carroll, "An automated reference frame selection (arfs) algorithm for cone imaging with adaptive optics scanning light ophthalmoscopy," Transl. Vis. Sci. & Technol. **6**, 9 (2017).

16. A. de Castro, G. Huang, L. Sawides, T. Luo, and S. A. Burns, "Rapid high resolution imaging with a dual-channel scanning technique," Opt. Lett. **41**, 1881–1884 (2016).

17. B. Gu, X. Wang, M. D. Twa, J. Tam, C. A. Girkin, and Y. Zhang, "Noninvasive in vivo characterization of erythrocyte motion in human retinal capillaries using high-speed adaptive optics near-confocal imaging," Biomed. Opt. Express **9**, 3653–3677 (2018).

18. Z. Zhong, B. L. Petrig, X. Qi, and S. A. Burns, "In vivo measurement of erythrocyte velocity and retinal blood flow using adaptive optics scanning laser ophthalmoscopy," Opt. Express **16**, 12746–12756 (2008).

19. P. Bedggood and A. Metha, "Analysis of contrast and motion signals generated by human blood constituents in capillary flow," Opt. Lett. **39**, 610–613 (2014).

20. E. Gofas-Salas, P. Mecê, C. Petit, J. Jarosz, L. M. Mugnier, A. M. Bonnefois, K. Grieve, J. Sahel, M. Paques, and S. Meimon, "High loop rate adaptive optics flood illumination ophthalmoscope with structured illumination capability," Appl. Opt. **57**, 5635–5642 (2018).

21. J. Lu, B. Gu, X. Wang, and Y. Zhang, "High-speed adaptive optics line scan confocal retinal imaging for human eye," PloS one **12**, e0169358 (2017).

22. S. Meimon, E. G. Salas, P. Mecê, K. Grieve, J. A. Sahel, and M. Paques, "Manipulation of the illumination geometry on adaptive optics (ao) flood illumination ophthalmoscope (fio) for dark field imaging of the retina," Investig. Ophthalmol. & Vis. Sci. **59**, 4641 (2018).

23. G. Ramaswamy and N. Devaney, "Pre-processing, registration and selection of adaptive optics corrected retinal images," Ophthalmic Physiol. Opt. **33**, 527–539 (2013).

24. D. Gratadour, L. Mugnier, and D. Rouan, "Sub-pixel image registration with a maximum likelihood estimator-application to the first adaptive optics observations of arp 220 in the L' band," Astron. & Astrophys. **443**, 357–365 (2005).

25. L. Tian and L. Waller, "Quantitative differential phase contrast imaging in an led array microscope," Opt. Express **23**, 11394–11403 (2015).

26. E. Meixner and G. Michelson, "Measurement of retinal wall-to-lumen ratio by adaptive optics retinal camera: a clinical research," Graefe's Arch. for Clin. Exp. Ophthalmol. **253**, 1985–1995 (2015).

27. R. Skalak and P. Branemark, "Deformation of red blood cells in capillaries," Science **164**, 717–719 (1969).

28. A. Guevara-Torres, A. Joseph, and J. Schallek, "Label free measurement of retinal blood cell flux, velocity, hematocrit and capillary width in the living mouse eye," Biomed. Opt. Express **7**, 4228–4249 (2016).

29. P. Mecê, E. Gofas-Salas, C. Petit, K. Grieve, C. Chabrier, M. Paques, and S. Meimon, "High ao-loop rate improves axial resolution in ao ophthalmoscopes," ARVO Imaging Eye Conf. (2018).

30. A. Nakano, Y. Sugii, M. Minamiyama, and H. Niimi, "Measurement of red cell velocity in microvessels using particle image velocimetry (piv)," Clin. Hemorheol. Microcirc. **29**, 445–455 (2003).